Bioorganic & Medicinal Chemistry 22 (2014) 5476–5486

Contents lists available at ScienceDirect

Bioorganic & Medicinal Chemistry

journal homepage: www.elsevier.com/locate/bmc

Love–Hate ligands for high resolution analysis of strain in ultra-stable protein/small molecule interaction

Michael Fairhead [a,†], Di Shen [b,†], Louis K. M. Chan [b], Ed D. Lowe [a], Timothy J. Donohoe [b,*], Mark Howarth [a,*]

[a] Department of Biochemistry, University of Oxford, South Parks Road, Oxford OX1 3QU, UK
[b] Department of Chemistry, University of Oxford, Chemistry Research Laboratory, 12 Mansfield Road, Oxford OX1 3TA, UK

ARTICLE INFO

Article history:
Received 12 May 2014
Revised 16 July 2014
Accepted 17 July 2014
Available online 24 July 2014

Keywords:
Protein crystallization
Biotin
Avidin
Mechanobiology
Chemical biology

ABSTRACT

The pathway of ligand dissociation and how binding sites respond to force are not well understood for any macromolecule. Force effects on biological receptors have been studied through simulation or force spectroscopy, but not by high resolution structural experiments. To investigate this challenge, we took advantage of the extreme stability of the streptavidin–biotin interaction, a paradigm for understanding non-covalent binding as well as a ubiquitous research tool. We synthesized a series of biotin-conjugates having an unchanged strong-binding biotin moiety, along with pincer-like arms designed to clash with the protein surface: 'Love–Hate ligands'. The Love–Hate ligands contained various 2,6-di-*ortho* aryl groups, installed using Suzuki coupling as the last synthetic step, making the steric repulsion highly modular. We determined binding affinity, as well as solving 1.1–1.6 Å resolution crystal structures of streptavidin bound to Love–Hate ligands. Striking distortion of streptavidin's binding contacts was found for these complexes. Hydrogen bonds to biotin's ureido and thiophene rings were preserved for all the ligands, but biotin's valeryl tail was distorted from the classic conformation. Streptavidin's L3/4 loop, normally forming multiple energetically-important hydrogen bonds to biotin, was forced away by clashes with Love–Hate ligands, but Ser45 from L3/4 could adapt to hydrogen-bond to a different part of the ligand. This approach of preparing conflicted ligands represents a direct way to visualize strained biological interactions and test protein plasticity.

© 2014 Elsevier Ltd. All rights reserved.

1. Introduction

Many effects in biology depend on force, including sensing of faithful chromosome segregation,[1] restraining cancer cell proliferation,[2] and adaptation to exercise.[3,4] Some of the forces involved in these events have been measured and key components for transducing and responding to force determined.[3] However, there are still major questions at the molecular level as to how force changes structure and reactivity. Force spectroscopy, particularly Atomic Force Microscopy (AFM), can identify how the energy barriers to ligand dissociation from biological receptors vary according to the pulling rate, as well as providing a distance from the ground state to the transition state for unbinding.[5] Nevertheless it is very difficult to reconcile these values with specific molecular features. Simulation has been important in bridging this gap, suggesting that there are new molecular interactions made as ligands are extracted from the binding site by an external force.[6,7] However, there has been limited experimental verification of such analyses. Also, simulation has often used simplifications to binding partners, as well as time-scales of unbinding that are orders of magnitude faster than occur in the cell.[6–8] This time-scale difference can distort the energy landscape, leading to the disappearance of energy barriers which would be significant at lower pulling rates.[5,9,10]

X-ray crystallography is the most widely used method for high resolution analysis of ligand binding interactions, but it is not possible to apply force directly to every ligand in the X-ray beam. Here through the synthesis of a series of chemical probes, we aimed to use crystallography to gain molecular insight into how force affected ligand interaction. We made use of the streptavidin–biotin system, a pinnacle of molecular recognition. Streptavidin is a protein with an affinity for the vitamin biotin of 4×10^{-14} M.[8] As well as being a favored model system, streptavidin is one of the most widely applied linkages or bridges in bioorganic chemistry and biotechnology.[11] There is extensive study of this system from

Abbreviations: D, Dead, non-binding streptavidin mutant; EC_{50}, half-maximal effective concentration; L3/4, loop connecting β-strands 3 and 4; LH, Love–Hate ligand; rmsd, root mean square deviation; SA, wild-type core streptavidin; SAe, core streptavidin with C-terminal hexaglutamate tag.

* Corresponding authors. Tel.: +44 (0)1865 275649; fax: +44 (0)1865 285002 (T.J.D.); tel.: +44 (0)1865 613233; fax: +44 (0)1865 613201 (M.H.).
E-mail addresses: timothy.donohoe@chem.ox.ac.uk (T.J. Donohoe), mark.howarth@bioch.ox.ac.uk (M. Howarth).

† These authors contributed equally.

http://dx.doi.org/10.1016/j.bmc.2014.07.029
0968-0896/© 2014 Elsevier Ltd. All rights reserved.

site-directed or random mutagenesis, AFM, and simulation; also streptavidin's symmetry and rigidity make it favorable for high-resolution crystallography.[6,9,11–14] Streptavidin's affinity for biotin relates to a hydrophobic cage around biotin, extensive van der Waals interactions, and a network of cooperative hydrogen bonds.[14] Hydrogen bonds to biotin include those from the loop between β-strands 3 and 4 (L3/4) of streptavidin. In the absence of biotin, L3/4 is commonly disordered and/or shows high temperature factors; L3/4 closes over the valeryl tail in all structures where biotin analogs or biotin conjugates are bound.[13–15]

We synthesized a tailored series of biotin conjugates, Love–Hate (LH) ligands, designed to leave the biotin core *unmodified*, so that specific interactions with the receptor could be retained, but to introduce a repulsive element through steric clash at positions distant to the binding site (Fig. 1). Using the series of LH ligands, as well as exploiting our orientation-controlled divalent streptavidin tetramers,[16] we gained insight into strain within ligand complexes through X-ray crystallography and equilibrium binding analysis.

2. Results

2.1. Design and synthetic route to the first Love–Hate ligand

We required ligands with the appropriate balance of attraction (through an unmodified biotin core) versus repulsion (through groups pointing back towards the protein, designed to introduce a broad van der Waals clash adjacent to the binding site) (Fig. 1A). The biotin core must be unmodified, in order to avoid interrupting the fundamental interactions with streptavidin (hydrogen bonding network shown in Figure 1B).[13,14] We avoided having a large group within one or two atoms from the biotin side-chain carbonyl, based on prior insight into such biotin conjugates designed to be resistant to biotinidase cleavage.[17,18] We also required ligands to have sufficient aqueous solubility for soaking into crystals to achieve high occupancy. We sought to avoid heterogeneity in ligand position, to help the ligand be resolved in the crystal structure and so that ligand strain would be at the same point on the protein in all of the unit cells. Ligands were designed to have ready synthetic accessibility, as well as to have a highly modular synthesis, through varying the di-*ortho* aryl groups to tune streptavidin repulsion (Fig. 1C).

Initially, we designed the ligand LH1, which contains an ethylene diamine spacer between biotin and a sterically hindered 2,6-diarylbenzene moiety (Fig. 1C). LH1 was assembled from commercially available benzoic acid (**1**) (Scheme 1A) that underwent C–H diiodination using $Pd(OAc)_2$ and I_2 with $PhI(OAc)_2$ as oxidant to give (**2**) in 74% yield.[19] 2,6-Diiodobenzoic acid (**2**) was then coupled with *N*-Boc ethylenediamine (**3**) under amide coupling conditions using EDC·HCl and HOBt, to give amide (**4**) in 56% yield. Next, Suzuki cross coupling with $PhB(OH)_2$ was then successfully

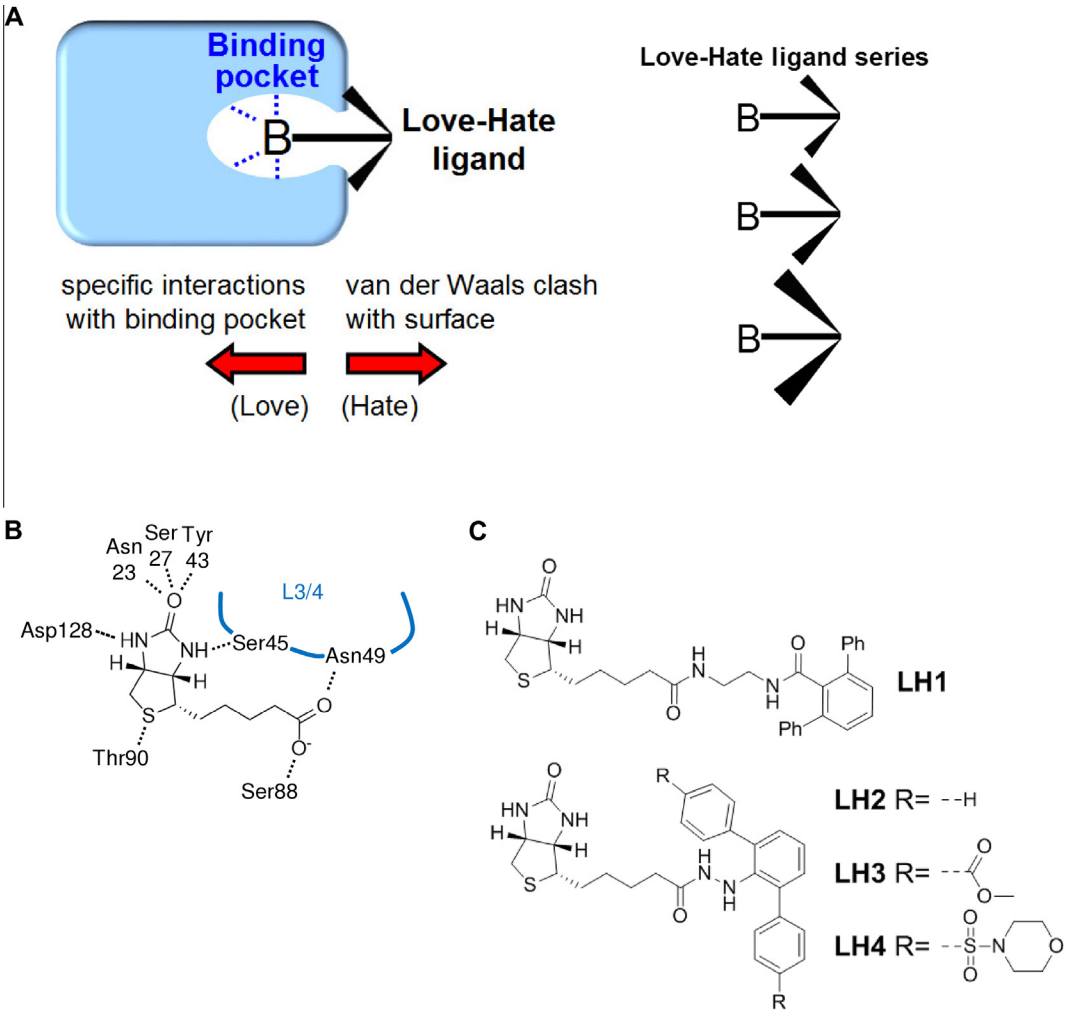

Figure 1. Principle and chemical structures of Love–Hate ligands. (A) Cartoon of strategy for ligand design. Protein in blue. B represents the high affinity ligand and dotted lines the stabilizing polar interactions. (B) Hydrogen-bonding contacts made by streptavidin to biotin, shown as dotted lines, with the Loop between strands 3 and 4 (L3/4) in blue. (C) Love–Hate (LH) ligand structures 1–4.

performed on the hindered diiodide (**4**).[20] The crude material was directly treated with trifluoroacetic acid for the deprotection of the Boc group, which subsequently allowed final amide coupling onto biotin NHS ester, to afford LH1 in 16% yield over 3 steps. LH1 identity and purity were validated by mass spectrometry (Section 4.1) and NMR (Supplementary methods).

2.2. Crystal structure of streptavidin bound to LH1

Streptavidin forms a dimer of dimers as its quaternary structure, with each subunit a β-barrel of 8 antiparallel β-strands.[13,14] LH1 gave a 1.1 Å structure in complex with streptavidin, with both binding sites in the asymmetric unit containing well defined ligand (Table 1, Fig. 2A and B and Supplementary Fig. S1). Despite the di-*ortho* phenyl groups, L3/4 of streptavidin was shut and all hydrogen bond contacts to biotin were preserved, with minimal difference to complexes with biotin itself,[14] and an extra potential hydrogen bond from LH1 to Ser112 (Fig. 2C and D).

Since the ethylene diamine spacer of LH1 allowed flexibility in positioning of the repulsive moieties, we designed ligands LH2–4, which have a linker three atoms shorter between biotin and the sterically hindered group (Fig. 1C).

2.3. Synthetic route to second series of Love–Hate ligands

The synthesis of the second series of Love–Hate ligands, LH2–4, utilized a similar cross-coupling strategy, but with diversification of the sterically hindered groups using cross coupling at the latest stage possible (Scheme 1B). Commercially-available 2,6-dibromoaniline (**5**) was treated with $NaNO_2$ to generate the diazonium salt and was reduced in situ to the 2,6-dibromohydrazine (**6**) using $SnCl_2$.[21] With hydrazine (**6**) in hand, we found that amide coupling with biotin under EDC·HCl and HOBt in DMF provided the optimal conditions, since hydrazide (**7**) directly precipitated out of solution upon completion of the reaction. Finally, Suzuki coupling, without extensive optimization, afforded the bulky LH2 ligand in 18% yield. LH3 and LH4 were prepared by the same route using the corresponding aryl boronic acids. The structure and purity of LH2, LH3 and LH4 were validated by mass spectrometry (Section 4.1) and NMR (Supplementary methods). Given the limited aqueous solubility of LH1, LH2 and LH3 (<2 mM in 10% DMSO), when further increasing the size of the adjunct rings in designing LH4, to favor solubility we used a substituent with multiple heteroatoms, sulfonylmorpholinyl. LH4 retained similar solubility in 10% DMSO to the other LH ligands.

2.4. Crystal structures of streptavidin bound to second series of Love–Hate ligands

Crystallization trials were set up with the second series of LH ligands. Despite several attempts we could not obtain a well-resolved crystal structure of LH2. With wild-type streptavidin we observed low ligand occupancy for LH2, complicated by twinning. Therefore we used our *trans*-divalent streptavidin, where only the 1 and 3 subunits on opposite sides of the tetramer could bind biotin ligands (Supplementary Fig. S2),[16] so avoiding any clash between adjacent ligands. The other two subunits were 'Dead', through three mutations to key biotin binding residues.[22] Such mixed tetramers can be readily generated by refolding from inclusion bodies a combination of Alive and Dead subunits. As a result of

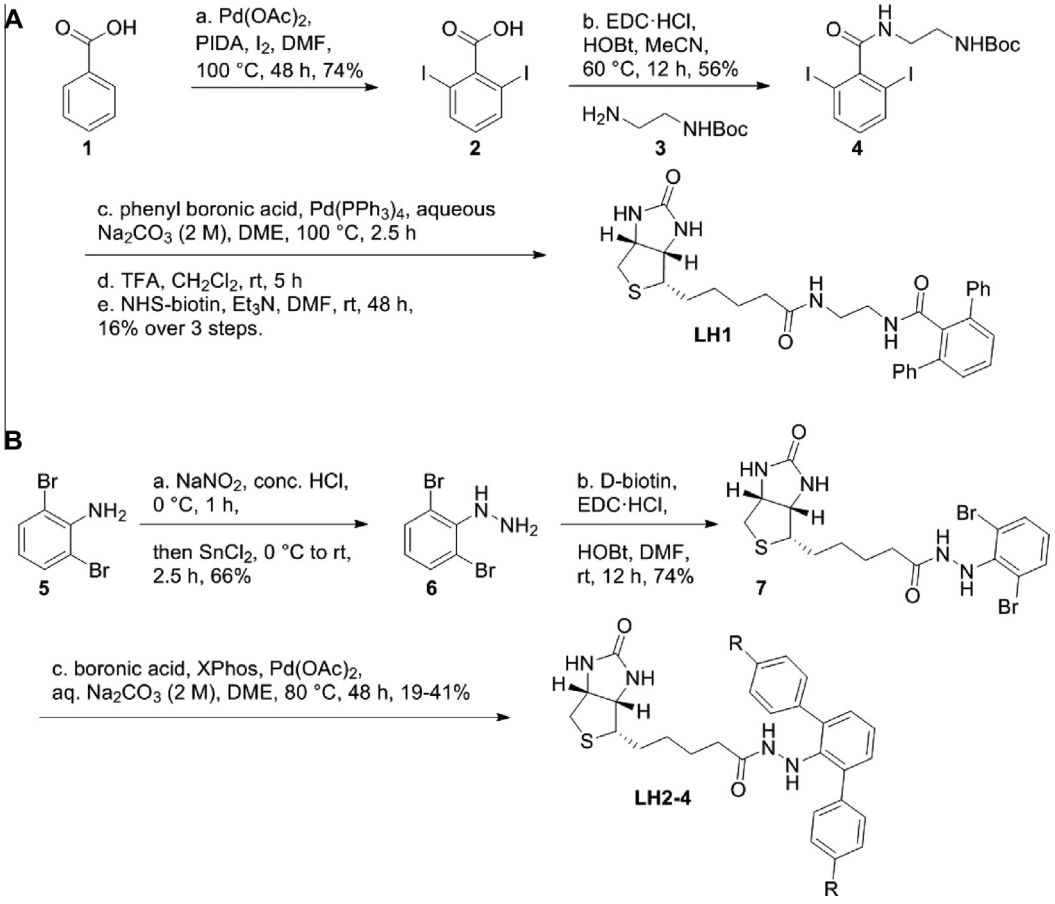

Scheme 1. Chemical synthesis route of Love–Hate ligand 1 (A) and Love–Hate ligands 2–4 (B).

Table 1
Data collection, refinement statistics, and structure validation for the Love–Hate ligand/Streptavidin structures

Data collection	SA-LH1 (PDB 4CPE)	SA-LH3 (PDB 4CPF)	*trans*-Divalent SA-LH4 (PDB 4CPH)	A86D SA-LH4 (PDB 4CPI)
Space group	I222	I222	C121	C121
Asymmetric unit	Dimer	Dimer	Tetramer	Tetramer
Unit cell size (Å)	46.59 × 93.93 × 104.32	47.08 × 94.12 × 104.79	90.74 × 47.49 × 104.88	81.26 × 81.25 × 90.69
Unit cell angles (°)	90 × 90 × 90	90 × 90 × 90	90 × 101.14 × 90	90 × 103.84 × 90
Completeness (%)*	93.1 (55.0)	93.0 (65.1)	96.6 (95.5)	99.6 (99.6)
Multiplicity	5.8 (3.2)	6.1 (2.4)	3.3 (3.2)	3.3 (3.3)
Refinement				
Resolution range (Å)	1.06–20.37	1.14–32.75	1.64–41.90	1.54–39.45
Total reflections	557,763 (17,822)	477,826 (13,372)	172,843 (16,293)	280,431(28,198)
Unique reflections	96,250 (5,646)	79,019 (5,486)	52,123 (5,108)	84,162 (8,419)
Mean I/sigma(I)	18.14 (2.46)	18.81 (2.83)	8.35 (1.93)	15.61 (2.34)
R-merge	0.0472 (0.4556)	0.0524 (0.339)	0.0788 (0.593)	0.0512 (0.622)
R_{work}/R_{free}	0.132/0.154	0.138/0.165	0.200/0.232	0.157/0.182
No. of atoms	2,165	2,224	4,069	4,355
Protein	1,861	1,955	3,709	3,846
Heteroatoms	78	43	106	198
Water	226	226	254	311
B factors (mean of all atoms, Å^2)				
Wilson Plot	9.73	11.68	18.96	17.55
Mean B value	15.00	18.60	28.60	25.10
Rmsd				
Bond length (Å)	0.011	0.010	0.009	0.008
Bond angle (Å)	1.42	1.39	1.23	1.17
LH ligand occupancy	0.83/0.81	0.82	0.83/0.86	0.92/0.91
LH ligand density correlation	0.91/0.95	0.96	0.83/0.82	0.95/0.95
Structure factors				
MolProbity clashscore	2.17 (97th percentile)	2.33 (96th percentile)	3.28 (98th percentile)	0.9 (99th percentile)
Poor rotamers (%)	1.08	0.51	1.35	1.28
Ramachandran outliers (%)	0	0	0	0
Ramachandran favored (%)	97.55	96.48	97.73	98.19
MolProbity score	1.11 (95th percentile)	1.24 (90th percentile)	1.28 (98th percentile)	0.86 (100th percentile)
Residues with bad bonds (%)	0.00	0.00	0.00	0.00
Residues with bad angles (%)	0.00	0.00	0.00	0.00

Statistics for the highest resolution shell are shown in parenthesis.
* Completeness for the highest resolution shells of SA-LH1 and SA-LH3 were lower than expected due to some spots diffracting beyond the boundaries of the detector. The highest resolution shells with high completeness for SA-LH1 are 1.16–1.18 Å (98%) and 1.26–1.28 Å (99%) for SA-LH3.

the Glu_6 tag on the Alive subunits, the mixed tetramers can subsequently be separated using anion exchange chromatography into forms with a defined number and orientation of functional biotin binding sites.[16] Unfortunately, despite dealing with the high levels of twinning, we were still unable to resolve clear density for the LH2 ligands.

However, we were able to obtain a 1.1 Å resolution crystal structure for LH3 bound to wild-type streptavidin. In one subunit, LH3 was clearly resolved in all its regions (Fig. 3A and B and Supplementary Fig. S3). The ligand had strikingly distorted the binding site, displacing L3/4 of streptavidin and preventing Asn49 and Ser88 forming polar contacts with biotin (Fig. 3C and D). The conformation of the rings had led the carbonyl of the methoxyester to bend back within hydrogen bonding distance of the *cis*-NH of biotin. Normally the *cis*-NH of biotin hydrogen-bonds to Ser45 (Fig. 1B), but the displaced Ser45 may be able to form an alternative hydrogen bond to the carbonyl of this same methoxyester (Fig. 3C and D). The guanidino of Arg84 was well positioned for a putative cation–π interaction[23] with the central phenyl ring of LH3 (Supplementary Fig. S3E).

LH4, with the largest headgroup on each phenyl ring, sulfonylmorpholinyl, did not yield crystals with wild-type streptavidin. However, LH4 was able to form crystals with *trans*-divalent streptavidin at 1.6 Å resolution. The density of the biotin core of LH4 was well resolved (Fig. 3A and B). Part of the central phenyl ring and one of the pendant phenyl rings of LH4 were seen clearly but the rest of LH4 had substantial disorder (Fig. 3B and Supplementary Fig. S4). LH4 also yielded major changes to the binding site: L3/4 was displaced and LH4 failed to form hydrogen bonds to three residues normally hydrogen-bonding to biotin (Ser45, Asn49 and Ser88) (Fig. 3C and D).

Examining the water molecules resolved within 4 Å of the bound ligand, there was no clear change for SA/LH1 as compared to SA/biotin. However in the case of LH3, the bending over of L3,4 led to two water molecules being resolved at the streptavidin/ligand interface, forming a variety of polar contacts (2023, 2053, CHAIN B). *trans*-Divalent SA/LH4 had only one extra water molecule resolved at the streptavidin/ligand interface (2010, CHAIN C), although this structure was solved at lower resolution.

2.5. Binding strength of Love–Hate ligand series

We characterized the dissociation constant of the ligand series for streptavidin. The exceptional affinity and stability of the biotin/streptavidin interaction mean that many standard assays are unsuitable, including surface plasmon resonance and isothermal titration calorimetry. Also the amount of ligand available from the multi-step syntheses prohibited certain approaches. We obtained relative K_d values using an equilibrium competition assay, based on the amount of biotin-4-fluorescein dissociation at increasing ligand concentration. The fluorescence of biotin-4-fluorescein is quenched ~90% upon binding to streptavidin, while fluorescence is regained upon release.[24] To avoid any interaction between bulky ligands binding to adjacent streptavidin binding sites, ligand binding was tested on a monovalent streptavidin (SAe1D3) with three subunits which do not bind biotin and one subunit that binds biotin with wild-type affinity.[16,22] Biotin itself was used in the assay as a reference ligand, with K_d of

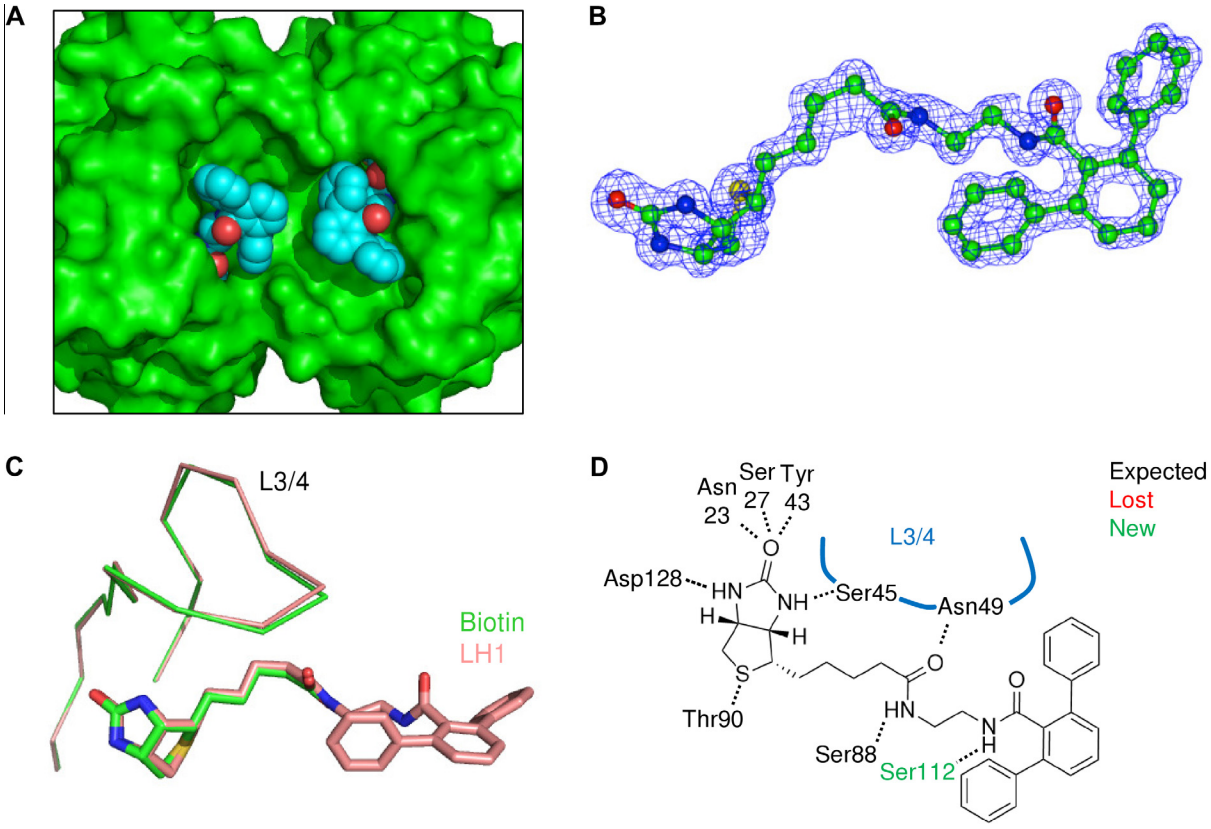

Figure 2. Crystal structure of streptavidin bound to LH1. (A) Crystal structure of adjacent binding sites in a streptavidin tetramer bound to LH1. Streptavidin is shown in green with a surface representation. LH1 is shown as its van der Waals surface, with carbons in cyan. (B) 2mFo-DFc electron density of LH1 (from chain B) contoured at 1 σ (blue) and cropped to within 1.5 Å of ligand atoms, overlaid with the ligand structure in stick format (green). (C) Overlay of biotin and the streptavidin L3/4 loop (green, from PDB 3RY2) with the equivalent part from the LH1/streptavidin structure (pink). Ligands are shown in stick format and protein in ribbon format. (D) Schematic of hydrogen bond network from streptavidin to LH1, with parental interactions to biotin in black, interactions lost for LH1 compared to biotin in red, and putative new interactions for LH1 in green.

4×10^{-14} M, as defined by Green, 1990.[8] Desthiobiotin was used as a weaker ligand, also of known affinity, ~100-fold weaker than biotin as reported by Hirsch and coworkers.[25] We confirmed that the assay had reached equilibrium by incubating for a further 2 days with no change in results. Despite the bulky substituents, LH1 showed minimal difference in equilibrium binding to biotin, with a 1.1-fold reduction in affinity (Table 2 and Supplementary Fig. S5A). LH2–4 showed reduced affinity compared to biotin (Table 2) but the effect was smaller than would be expected based on the major changes in the binding interface from the crystal structures. Also, the relative affinity was counter-intuitive, with LH4 showing stronger streptavidin binding than its smaller relative LH3 (Table 2).

Desiring to span a wider range of affinities, we explored the reasons for the reduced effect on affinity of such a sterically hindered biotin ligand. The degrees of freedom in LH2–4 still allow avoidance of much of the clash with streptavidin. Therefore we created an A86D streptavidin mutant to restrict this freedom. Steric clash of Asp86 was designed to direct a different orientation of the central phenyl ring of the Love–Hate ligand, so favoring the desired repulsive interactions from van der Waals clash of the diphenyl branches with the surface of streptavidin.

There is potential electrostatic repulsion between neighboring carboxylates of biotin and Asp86 within A86D streptavidin. Therefore biocytin (biotinyl-L-lysine) was used as a reference ligand for A86D streptavidin, giving a similar binding curve as biotin showed with wild-type streptavidin (Supplementary Fig. S5B). Biocytin and biotin were previously found to have equivalent affinity for wild-type streptavidin.[26] LH4 binding was greatly impaired compared to biocytin for A86D streptavidin, with a 150-fold decrease in binding (Table 2).

2.6. A86D streptavidin crystal structure with LH4

To understand an even more strained interaction (as judging from the measured EC_{50} value, Table 2) we solved the structure of the LH4 ligand bound to A86D streptavidin at 1.5 Å resolution (Table 1). The structure of the complex showed clear density for two of the four copies of LH4 present in the asymmetric unit (Fig. 4A and B and Supplementary Fig. S6). The pendant arms had a very different orientation for LH4/A86D streptavidin compared to LH4/*trans*-divalent streptavidin. The valeryl tail for LH4/A86D projected well away from the classic orientation for biotin (3.6 Å between the carbonyl carbons) (Fig. 4C). L3/4 was again displaced into an open conformation, with loss of Asn49 and Ser88 hydrogen bonds. However, novel putative hydrogen bonds were formed: from Asn85 to one of the sulfonyl groups, and from Asp86 to one of the hydrazide NH groups. As with the streptavidin/LH3 structure, Ser45 did not form the classic hydrogen bond to the *cis*-NH of the ureido ring, but in a new orientation Ser45 could form a putative hydrogen bond to the carbonyl of the valeryl tail. One of the sulfonyl oxygens was close enough to form an intra-ligand hydrogen bond to the *cis*-NH of biotin (Fig. 4C and D). Similar to the *trans*-divalent SA/LH4 structure, A86D SA/LH4 had one water molecule resolved at the streptavidin/ligand interface (2022, CHAIN D) that was not observed in SA/biotin structures.[13,27]

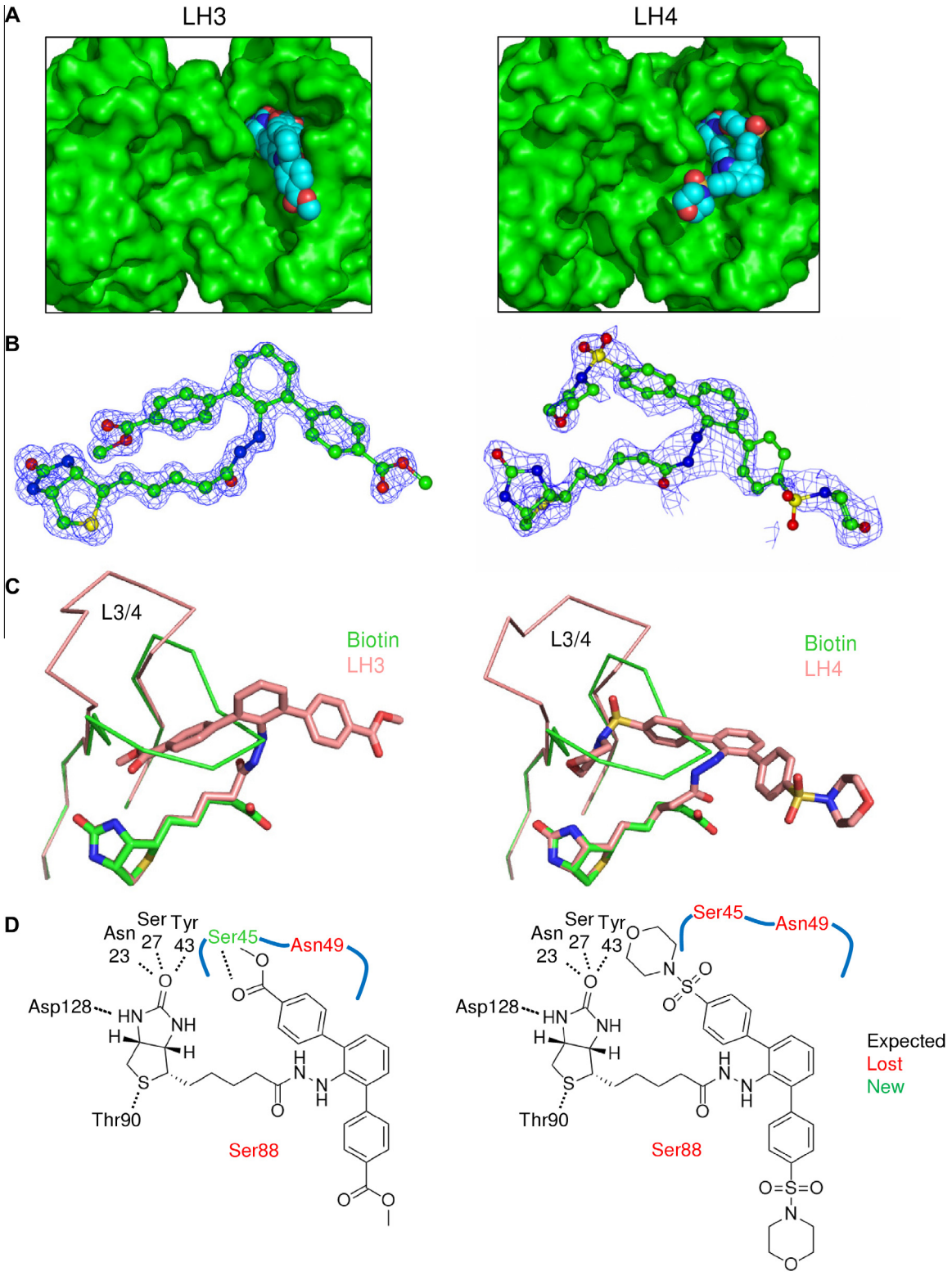

Figure 3. Crystal structures of streptavidin bound to LH3 or LH4. (A) Crystal structure of adjacent binding sites in a streptavidin tetramer bound to LH3 (left) or LH4 (right). Streptavidin is shown in green with a surface representation. LH3 or LH4 is shown as its van der Waals surface, with carbons in cyan. (B) 2mFo-DFc electron density of LH3 (left, from chain B) or LH4 (right, from chain C) contoured at 1 σ (blue) and cropped to within 1.5 Å of ligand atoms, overlaid with the ligand structure in stick format (green). (C) Overlay of biotin and the streptavidin L3/4 loop (green, from PDB 3RY2) with the equivalent part from the LH3 (left) or LH4 (right) streptavidin complex (pink). Ligands are shown in stick format and protein in ribbon format. (D) Schematic of hydrogen bond network from streptavidin to LH3 (left) or LH4 (right), with parental interactions to biotin in black, interactions lost for LH compared to biotin in red, and putative new interactions for LH in green.

Table 2
Competition assay for Love–Hate ligand binding affinity

Ligand	Biotin	Desthiobiotin	Lipoic acid	LH1	LH2	LH3	LH4	Biocytin A86D	LH4 A86D
EC_{50}, nM (95% CI)	28 (20–39)	5,410 (4,580–6,390)	n/a	31 (17–56)	251 (157–401)	178 (124–257)	138 (87.7–216)	19 (17–22)	2,840 (2,220–3,640)
R^2	0.98	0.99	n/a	0.94	0.96	0.98	0.96	0.99	0.97
Fold-decrease in affinity	1[a]	190	n/a	1.1	9	6.4	4.9	1[b]	150

Biotin-4-fluorescein was incubated with streptavidin and the indicated concentration of each ligand for 48 h at 37 °C and fluorescence was determined. The concentration of ligand for 50% dissociation of biotin-4-fluorescein (EC_{50}) was determined, along with the 95% confidence intervals (CI) for the EC_{50} and the correlation coefficient (R^2) for the fit. Lipoic acid served as a control, with no dissociation of biotin-4-fluorescein induced (n/a, not applicable). For wild-type streptavidin binding sites, the EC_{50} for the ligand was divided by the EC_{50} for biotin, to give a relative decrease in binding affinity. For A86D streptavidin binding sites, the EC_{50} for the ligand was divided by the EC_{50} for biocytin. The fluorescence curves are shown in Fig. S5. The one-site competitive binding fit was calculated using GraphPad Prism, giving an EC_{50} with 95% confidence intervals (CI) as well as a R^2 Pearson correlation coefficient value.

[a] Defined as 1 for all experiments with wild-type streptavidin.

[b] Defined as 1 for the experiments with streptavidin A86D.

2.7. Comparison of Love–Hate/streptavidin complex structures

Overlaying the Love–Hate ligand complex structures with the streptavidin/biotin structure, the organization of the ureido and thiophene rings of biotin in each structure was unchanged within error to biotin itself (Fig. 4E). Focusing on the L3/4 loop shows how the loop was shut with LH1, just as for biotin (Fig. 2C) but pushed into different open conformations in the presence of LH3 (Fig. 3C), LH4 (Fig. 3C) or LH4 bound to the A86D mutant (Fig. 4C). The valeryl tail was unchanged compared to biotin for LH1 but gradually more distorted from biotin in LH3, LH4 and LH4/A86D (Fig. 4E).

3. Conclusion

Here we have generated a modular series of ligands to introduce repulsion into an ultra-stable protein/small molecule interaction and analyzed these ligand/protein complexes at high resolution by X-ray crystallography. The four crystal structures show the plasticity of this outstanding ligand interaction. The hydrogen bonds surrounding the ureido and thiophene rings of biotin survived for all Love–Hate ligands but biotin's valeryl tail could change orientation and the L3/4 loop, previously considered essential for high affinity binding,[18,28,29] could be displaced by the Love–Hate ligand arms. A distortion of L3/4 has recently been suggested for avidin bound to a ferrocene-biotin conjugate.[30] In one subunit, L3/4 is closed. In the other observed subunit, L3/4 is disordered but the electron density for the ferrocene-biotin is weak,[30] so it is unclear whether L3/4 has been displaced by the ligand.

There has been substantial interest in making biotin conjugates resistant to biotinidase, an enzyme in blood which cleaves the amide bond to release biotin. Biotinidase interferes with clinical applications using streptavidin or avidin, such as pre-targeted radiotherapy in cancer.[31] For designed biotinidase-resistant conjugates, small changes adjacent to the biotin in a variety of cyanocobalamin conjugates (e.g., addition of a methyl group to the biotinamide nitrogen) caused large decreases in streptavidin binding affinity.[17,18] In contrast, the large arms on LH3 and LH4 caused gross disruption of the biotin binding site, with displacement of L3/4 and loss of multiple hydrogen bonding contacts to the biotin core, but with only small change in affinity. Point mutation of residues on L3/4 contacting biotin previously caused great loss of biotin binding affinity: S45A streptavidin has ~900-fold reduced affinity for biotin.[28] Also, based on structures of the low off-rate mutant traptavidin,[32] we previously identified Ser45 as a key determinant of biotin dissociation.[29] The effect of Asn49 or Ser88 mutation on biotin K_d has not been fully evaluated but circularly-permuted streptavidin lacking L3/4 had biotin affinity reduced more than a million-fold.[33,34] This discrepancy could be rationalized if LH2-LH4 formed extra hydrophobic contacts or hydrogen bonds. Potential new interactions (i.e., not present to biotin itself), including hydrogen bond or cation–π interactions, were found for LH3–4, including Ser45 interacting with different parts of the ligands. Given the surprising finding that LH3 and LH4 bind well to streptavidin even without many classic interactions of the biotin binding site, these ligands may serve as a foundation to create streptavidin mutants that bind well to such biotin conjugates, for clinical imaging and pre-targeted cancer radiotherapy and to overcome blocking by endogenous biotin in the bloodstream.[35] It is always possible that a crystal structure captures one out of various structural isoforms present in solution; interpretable occupancy of only half of the accessible binding sites in some of our structures suggests that other binding modes of LH ligands may be possible and will require future investigation.

Other structures have been solved for avidin or streptavidin in complex with reduced affinity ligands[36–40] but not with the sequential extension of the ligand series employed here for gradual introduction of repulsion. The crystal structure of the D128A streptavidin mutant bound to biotin showed that a water had filled the extra space occupied by the Asp128 head-group and the biotin was somewhat displaced from the wild-type structure.[41] With our ligands we found no replacement of contacts to the ureido groups by water molecules. This result is consistent with evidence from simulation that the cooperativity of the five hydrogen bonds to streptavidin from biotin's ureido group is central to the exceptional thermodynamic and mechanical stability of this interaction.[42] Relevant crystallographic insights to strained complexes also come from colicins trapped in a complex with non-cognate anti-toxins via a disulfide.[43] In addition, quantum mechanical calculations have shown that proteins do not always bind the lowest energy conformer of a small molecule ligand.[44]

It is a synthetic challenge to create ligands with the right balance of repulsion, rigidity and solubility. Covalent tethering of biotin onto streptavidin in such a way as to strain biotin binding might be possible. However, the large free-energy of biotin binding might instead trap a locally unfolded conformation of streptavidin at the tethering site, or promote inter-tetramer interactions and so aggregation. In future studies, it will be worth investigating even further repulsion in the streptavidin-biotin system and exploring the Love–Hate ligand approach in other biological systems where force changes function.[3,5] The modular nature of the synthetic route that was developed here should aid in the preparation of a wide variety of synthetic analogs to address these fundamental questions.

4. Experimental

4.1. Ligand synthesis

4.1.1. General synthetic methods

All solvents and reagents were used as commercially supplied, without extra precautions unless otherwise stated. All chemical reagents were from Sigma–Aldrich unless stated. Anhydrous chloroform and acetonitrile were dried by filtration through an

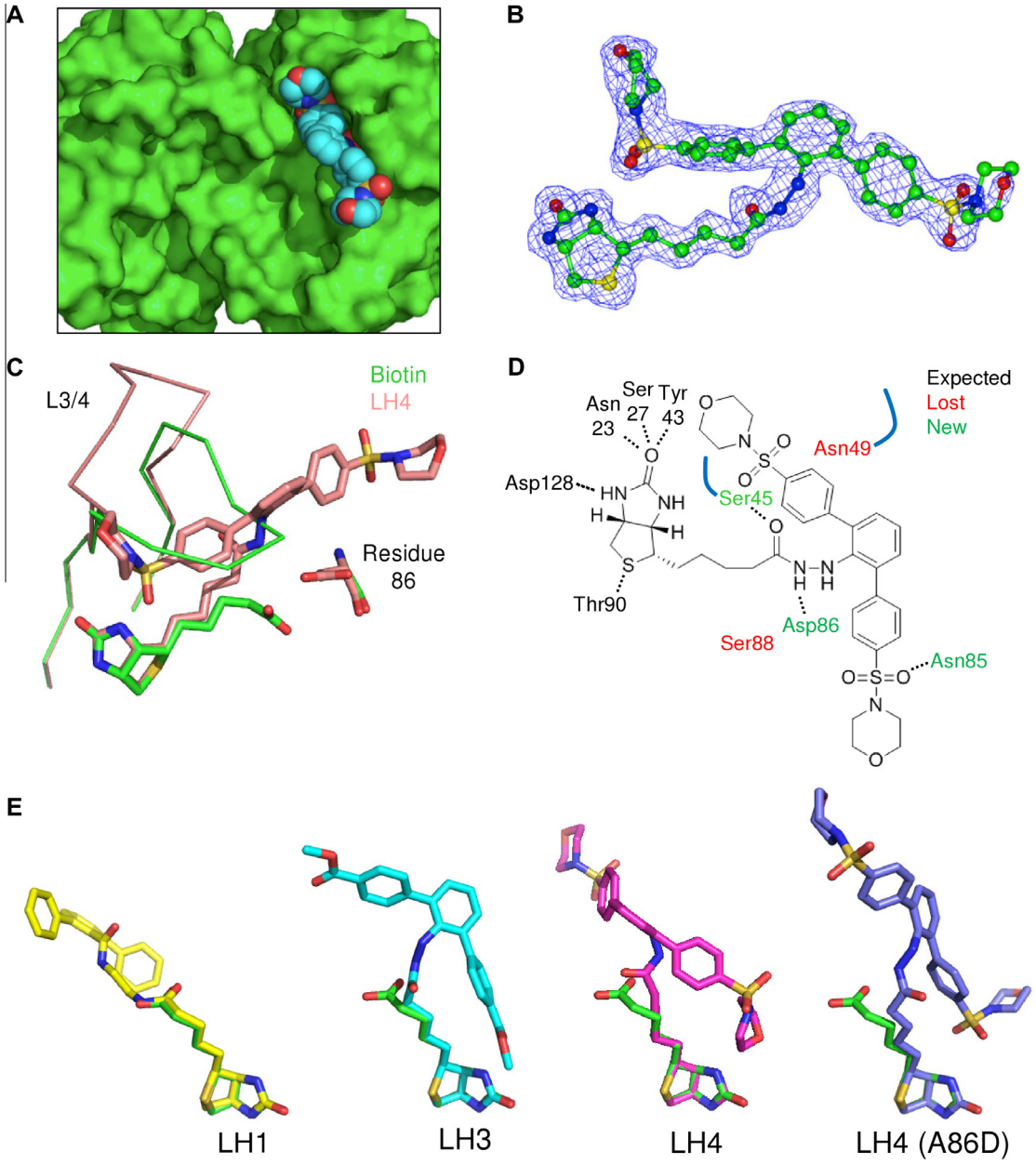

Figure 4. Crystal structure of A86D streptavidin bound to LH4. (A) Structure of adjacent binding sites in A86D streptavidin bound to LH4. A86D streptavidin is shown in green with a surface representation. LH4 is shown as its van der Waals surface, with carbons in cyan. (B) 2mFo-DFc electron density of LH4/A86D streptavidin (from chain D) contoured at 1 σ (blue) and cropped to within 1.5 Å of ligand atoms, overlaid with the ligand structure in stick format (green). (C) Overlay of biotin, the streptavidin L3/4 loop and residue 86 (green, from PDB 3RY2) with the equivalent part from the LH4/A86D streptavidin structure (pink). Ligands are shown in stick format. (D) Schematic of hydrogen bond network from A86D streptavidin to LH4, with parental interactions to biotin in black, interactions lost for LH4 compared to biotin in red, and putative new interactions for LH4 in green. (E) Comparison of all LH conformations. Overlay of conformation bound to wild-type streptavidin for biotin (in green, from PDB 3RY2) compared to LH1, LH3 and LH4. Biotin bound to wild-type streptavidin is also overlaid with LH4 bound to A86D streptavidin. Ligands are shown in stick format.

activated alumina purification column. Petrol refers to petroleum ether in the boiling range 30–40 °C. Flash column chromatography (FCC) was performed using Merck Kieselgel 60 silica (40–63 μm). ^{1}H nuclear magnetic resonance (NMR) spectra were recorded on a Bruker AV400 (400 MHz) or Bruker AVII500 (500 MHz). ^{13}C NMR spectra were recorded on a Bruker AV400 (101 MHz) or AVII500 (126 MHz) as stated. Chemical shifts (δ, in ppm) are reported relative to residual solvent peaks. Coupling constants are quoted to the nearest 0.1 Hz for ^{1}H NMR and to the nearest 1 Hz for ^{13}C NMR. Mass spectra under the conditions of electrospray ionization (ESI) were recorded on a Fisons Platform II analyzed using a Time of Flight system. Fourier transform infrared spectra (FTIR) were recorded as evaporated thin films on a Bruker Tensor 27 and analyzed by OPUS software. Melting points (MP) were obtained using a Leica VMTG heated-stage microscope and are uncorrected.

4.1.2. 2,6-Diiodobenzoic acid (2)

Benzoic acid (**1**) (500 mg, 4.09 mmol), $Pd(OAc)_2$ (45.9 mg, 0.20 mmol, Alfa Aesar), iodobenzene diacetate (PIDA) (2.00 g, 6.14 mmol) and I_2 (1.56 g, 6.14 mmol) were dissolved in DMF (20 mL) under argon in a sealed tube. The reaction mixture was stirred at 100 °C for 48 h, then cooled to rt, diluted with ethyl acetate (50 mL) and washed with aqueous HCl (1 M, 50 mL × 4). The organic phase was washed with brine, dried over Na_2SO_4 and concentrated in vacuo. The residue was recrystallized from ethyl

acetate and petrol (EtOAc/petrol, 10:1) to give the product as a light yellow solid (1.13 g, 74%). Melting point = 179–180 °C (Lit: 184–187 °C[45]); ^{1}H NMR (500 MHz, $CDCl_3$) δ 7.84 (d, J = 7.9 Hz, 2H), 6.82 (t, J = 7.9 Hz, 1H); ^{13}C NMR (126 MHz, $CDCl_3$) δ 172.5, 144.4, 138.7, 132.1, 90.7. Spectroscopic data are consistent with those previously reported.[19]

4.1.3. *tert*-Butyl (2-aminoethyl)carbamate (3)

A solution of di-*tert*-butyl dicarbonate (2.10 mL, 9.20 mmol) in chloroform (45 mL) was added via a syringe pump over 3 h to a solution of ethylenediamine (3.10 mL, 45.8 mmol) in chloroform (50 mL) at 0 °C. The reaction was stirred for 24 h at rt to give a white suspension which was then washed with saturated Na_2CO_3 (100 mL × 3). The organic layer was dried over Na_2SO_4 and concentrated in vacuo to yield the title compound, **3**, as a colorless oil (1.32 g, 90%); ^{1}H NMR (400 MHz, $CDCl_3$) δ 5.20 (br. s, 1H), 3.10 (m, 2H), 2.72 (m, 2H), 1.37 (s, 9H), 1.26 (br. s, 1H); ^{13}C NMR (101 MHz, $CDCl_3$) δ 156.2, 79.1, 43.4, 41.8, 28.4. Spectroscopic data are consistent with those previously reported.[46]

4.1.4. *tert*-Butyl (2-(2,6-diiodobenzamido)ethyl)carbamate (4)

tert-Butyl (2-aminoethyl)carbamate (**3**, 400 mg, 2.50 mmol), 2,6-diiodobenzoic acid (**2**, 778 mg, 2.08 mmol), *N*-(3-dimethylaminopropyl)-*N*′-ethylcarbodiimide hydrochloride (EDC·HCl, 399 mg, 2.08 mmol, Fluorochem) and 1-hydroxybenzotriazole (HOBt, 281 mg, 2.08 mmol, Alfa Aesar) were dissolved in MeCN (25 mL) in a sealed tube and the reaction was stirred at 60 °C for 12 h. The crude mixture was filtered through a short pad of silica gel, eluted with ethyl acetate, then recrystallized with dichloromethane to yield the product, **4**, as a white solid (600 mg, 56%). Melting point = 74–75 °C; ν_{max} (thin film)/cm^{-1} 3351, 3256, 2976, 2931, 2160, 2029, 766, 689; ^{1}H NMR (500 MHz, $CDCl_3$) δ 7.73 (d, J = 7.9 Hz, 2H), 6.70 (br. s, 1H), 6.68 (t, J = 7.9 Hz, 1H), 5.20 (br. s, 1H), 3.55 (m, 2H), 3.42 (m, 2H), 1.39 (s, 9H); ^{13}C NMR (126 MHz, $CDCl_3$) δ 170.4, 156.6, 147.0, 138.8, 131.6, 92.2, 79.6, 40.7, 39.8, 28.4; High Resolution Mass Spectrometry (HRMS) (ESI$^+$) calculated for $[C_{14}H_{18}I_2N_2O_3+Na]^+$ 538.9299, found 538.9278 (Δ 3.9 ppm).

4.1.5. Biotinamidoethyl-[1,1′:3′,1″-terphenyl]-2′-carboxamide (LH1)

tert-Butyl (2-(2,6-diiodobenzamido)ethyl)carbamate (**4**, 50.0 mg, 0.0969 mmol), phenyl boronic acid (35.4 mg, 0.290 mmol), $Pd(PPh_3)_4$ (11.2 mg, 0.00969 mmol, Strem Chemicals), aqueous Na_2CO_3 (2 M, 1 mL, Acros) and 1,2-dimethoxyethane (4 mL) were placed in a sealed tube, and the mixture was degassed with argon. The reaction mixture was then heated at 100 °C for 2.5 h, allowed to cool to rt, filtered through a short pad of silica gel, eluted with diethyl ether, and concentrated in vacuo. The crude material was redissolved in dichloromethane (0.3 mL) and TFA (74 μL, 1 mmol) was added. The yellow solution was stirred at rt for 5 h, concentrated in vacuo and then redissolved in DMF (0.3 mL) before D-biotin *N*-hydroxysuccinimide ester (33.1 mg, 0.0969 mmol), and triethylamine (176 μL, 1.26 mmol) were added. The mixture was further stirred at rt for 48 h and purified via column chromatography (CH_2Cl_2/MeOH, 9:1) to afford the product, LH1, as a white solid (8.2 mg, 16%). Melting point = 134–136 °C; $[\alpha]_D^{20}$ +27.2 (*c* 0.25, $CHCl_3$); ν_{max} (thin film)/cm^{-1} 3313, 2925, 1697, 1647, 1541, 1457, 761, 702; ^{1}H NMR (500 MHz, MeOD) δ 7.56 (m, 1H), 7.48 (m, 2H), 7.44–7.39 (m, 5H), 6.91 (br. s, 1H), 4.50 (dd, J = 7.7, 4.6 Hz, 1H), 4.30 (dd, J = 7.9, 4.4 Hz, 1H), 3.20 (m, 1H), 2.98 (m, 2H), 2.93 (dd, J = 12.8, 4.9 Hz, 1H), 2.84 (m, 2H), 2.72 (d, J = 12.6 Hz, 1H), 2.07 (t, J = 7.6 Hz, 2H), 1.75–1.39 (m, 6H); ^{13}C NMR (126 MHz, MeOD) δ 176.0, 172.4, 166.1, 142.0, 141.5, 136.9, 130.2, 130.2, 130.0, 129.3, 128.7, 63.4, 61.6, 57.0, 41.1, 39.9, 39.7, 36.8, 29.8, 29.5, 26.6; HRMS (ESI$^+$) calculated for $[C_{31}H_{34}N_4O_3S+Na]^+$ 565.2244, found 565.2223(Δ 3.7 ppm).

4.1.6. 2,6-Dibromophenylhydrazine (6)

Glassware was washed with diethyl ether before use. A solution of $NaNO_2$ (276 mg, 4.00 mmol) in H_2O (1.7 mL) was added dropwise to a white suspension of 2,6-dibromoaniline (**5**) (500 mg, 2.00 mmol) in aqueous HCl (37%, 5 mL) while cooling with an ice-water bath. The reaction mixture was stirred at 0 °C for 1 h to give a yellow suspension. Then a solution of $SnCl_2$ (760 mg, 4.00 mmol) in aqueous HCl (37%, 1.2 mL) was added dropwise at 0 °C. The reaction was stirred for 30 min before being warmed to rt and further stirred for 2 h to give a thick yellow suspension. The reaction was cooled to 0 °C, and solid sodium hydroxide was added until the pH was 9. The resulting yellow suspension was extracted with diethyl ether, dried over Na_2SO_4, concentrated in vacuo, and purified via column chromatography (petrol/ether, 9:1) to afford the product, **6**, as a yellow solid (354 mg, 66%). **6** was highly reactive towards acetone, ethyl acetate and acetonitrile; decomposition was also observed in methanol. Thus, careful handling was crucial to obtain pure material. Melting point = 79–82 °C; ν_{max} (thin film)/cm^{-1} 3228, 2416, 1427, 755, 716, 658; ^{1}H NMR (400 MHz, MeOD) δ 7.60 (d, J = 8.1 Hz, 2H), 6.92 (t, J = 8.0 Hz, 1H), 4.91 (br s, 3H); ^{13}C NMR (101 MHz, MeOD) δ 145.1, 132.7, 126.1, 117.6; HRMS (ESI$^+$) calculated for $[C_6H_6Br_2N_2+H]^+$ 264.8970, found 264.8981 (Δ −3.2 ppm).

4.1.7. *N*′-(2,6-Dibromophenyl)-biotinyl hydrazide (7)

2,6-Dibromophenylhydrazine (**6**, 302 mg, 1.14 mmol), D-biotin (185 mg, 0.757 mmol, Fluorochem), *N*-(3-dimethylaminopropyl)-*N*′-ethylcarbodiimide hydrochloride (218 mg, 1.14 mmol, Fluorochem), and HOBt (154 mg, 1.14 mmol, Alfa Aesar) were dissolved in DMF (15 mL). The yellow solution was stirred at rt for 18 h to give a white suspension which was then filtered to give the product, **7**, as a white solid (287 mg, 74%). Melting point = 168–170 °C; $[\alpha]_D^{20}$ +21.6 (*c* 0.25, MeOH); ν_{max} (thin film)/cm^{-1} 3269, 2929, 2360, 2341, 1696, 1440; ^{1}H NMR (500 MHz, MeOD) δ 7.53 (d, J = 8.2 Hz, 2H), 6.81 (t, J = 8.0 Hz, 1H), 4.50 (m, 1H), 4.29 (dd, J = 7.9, 4.4 Hz, 1H), 3.20 (ddd, J = 8.7, 6.0, 4.6 Hz, 1H), 2.94 (dd, J = 12.9, 5.0 Hz, 1H), 2.72 (d, J = 12.6 Hz, 1H), 2.25 (t, J = 7.2 Hz, 2H), 1.81–1.53 (m, 4H), 1.50–1.38 (m, 2H); ^{13}C NMR (126 MHz, MeOD) δ 175.0, 166.1, 144.4, 134.2, 125.6, 115.6, 63.3, 61.6, 57.0, 41.1, 34.2, 29.8, 29.4, 26.4; HRMS (ESI$^+$) calculated for $[C_{16}H_{20}Br_2N_4O_2S+Na]^+$ 512.9566, found 512.9553 (Δ 1.2 ppm).

4.1.8. General procedure for the Suzuki coupling

N′-(2,6-Dibromophenyl)-biotinyl hydrazide (**7**, 50.0 mg, 0.102 mmol, 1 equiv), the appropriate boronic acid (0.306 mmol, 3 equiv), $Pd(OAc)_2$ (1.1 mg, 0.00508 mmol, 0.05 equiv., Alfa Aesar), 2-dicyclohexylphosphino-2′,4′,6′-triisopropylbiphenyl (XPhos) (3.6 mg, 0.00765 mmol, 0.075 equiv), aqueous Na_2CO_3 (2 M, 0.32 mL, Acros), and 1,2-dimethoxyethane (0.64 mL) were placed in a sealed tube, and degassed with argon. The suspension was then heated at 80 °C for 48 h, and the crude mixture was directly purified by column chromatography (CH_2Cl_2/MeOH, 95:5).

4.1.9. *N*′-([1,1′:3′,1″-Terphenyl]-2′-yl)-biotinyl hydrazide (LH2)

Benzeneboronic acid (37.2 mg) was subjected to the general procedure for Suzuki coupling with **7** to give the title compound (LH2, 13.1 mg, 26%) as a yellow solid. Melting point = 111–112 °C; $[\alpha]_D^{20}$ +75.6 (*c* 0.25, $CHCl_3$); ν_{max} (thin film)/cm^{-1} 3254, 3057, 2929, 2860, 1701, 1455, 1420, 758, 703; ^{1}H NMR (500 MHz, $CDCl_3$) δ 7.56 (m, 4H), 7.47 (t, J = 7.7 Hz, 4H), 7.37 (m, 2H), 7.16 (m, 2H), 7.08 (m, 1H), 6.44 (br. s, 1H), 6.27 (br. s, 1H), 6.01 (br. s, 1H), 5.30 (br. s, 1H), 4.43 (m, 1H), 4.19 (m, 1H), 3.03 (m, 1H), 2.83 (dd, J = 12.8, 4.9 Hz, 1H) 2.63 (d, J = 12.6 Hz, 1H), 1.62–1.08 (m, 8H); ^{13}C NMR (126 MHz, $CDCl_3$) δ 171.3, 163.6, 142.8, 140.4, 131.2, 130.4, 129.0, 128.8, 127.3, 122.1, 61.7, 60.1,

55.3, 40.4, 33.2, 28.2, 28.0, 24.5; HRMS (ESI^+) calculated for $[C_{28}H_{30}N_4O_2S+Na]^+$ 509.1982, found 509.1974 (Δ 1.5 ppm).

4.1.10. Dimethyl 2′-(biotinyl)hydrazinyl)-[1,1′:3′,1″-terphenyl]-4,4″-dicarboxylate (LH3)

4-Methoxycarbonylphenyl boronic acid (54.0 mg) was subjected to the general procedure of Suzuki coupling with **7** to give the title compound (LH3, 11.6 mg, 19%) as a colorless solid. Melting point = 93–95 °C; $[\alpha]_D^{20}$ +28.8 (*c* 0.25, $CHCl_3$); ν_{max} (thin film)/cm^{-1} 3299, 2949, 2363, 2342, 1706, 1400, 1278; ^1H NMR (500 MHz, $CDCl_3$) δ 8.13 (d, *J* = 8.5 Hz, 4H), 7.65 (d, *J* = 8.5 Hz, 4H), 7.17 (m, 2H), 7.12 (m, 1H), 6.48 (d, *J* = 4.1 Hz, 1H), 6.20 (d, *J* = 4.4 Hz, 1H), 5.83 (br. s, 1H), 5.01 (br. s, 1H), 4.45 (dd, *J* = 7.6, 5.0 Hz, 1H), 4.21 (m, 1H), 3.95 (s, 6H), 3.02 (m, 1H), 2.88 (dd, *J* = 12.9, 5.0 Hz, 1H), 2.84 (d, *J* = 12.9 Hz, 1H), 1.67–1.12 (m, 8H); ^{13}C NMR (126 MHz, $CDCl_3$) δ 171.6, 166.9, 163.3, 145.2, 142.7, 130.8, 130.4, 130.1, 129.1, 129.0, 122.4, 61.7, 60.0, 55.3, 52.3, 40.4, 33.0, 28.2, 28.0, 24.6; HRMS (ESI^+) calculated for $[C_{32}H_{34}N_4O_6S+Na]^+$ 625.2091, found 625.2101 (Δ −1.5 ppm).

4.1.11. *N*′-(4,4″-Bis(morpholinosulfonyl)-[1,1′:3′,1″-terphenyl]-2′-yl)-biotinyl hydrazide (LH4)

4-(4-Morpholinylsulfonyl)phenylboronic acid (83.0 mg) was subjected to the general procedure for Suzuki coupling with **7** to give the title compound (LH4, 32.7 mg, 41%) as a yellow solid. Melting point = 162–165 °C; $[\alpha]_D^{20}$ +22.4 (*c* 0.25, $CHCl_3$); ν_{max} (thin film)/cm^{-1} 3326, 2921, 2859, 2247, 1698, 1165, 728; ^1H NMR (500 MHz, $CDCl_3$) δ 7.83 (d, *J* = 8.5 Hz, 4H), 7.75 (d, *J* = 8.5 Hz, 4H), 7.19–7.10 (m, 3H), 7.02 (br. s, 1H), 6.10 (br. s, 1H), 5.99 (br. s, 1H), 5.13 (br. s, 1H), 4.43 (dd, *J* = 7.6, 5.0 Hz, 1H), 4.21 (dd, *J* = 7.6, 4.7 Hz, 1H), 3.77 (m, 8H), 3.07 (m, 8H), 3.04 (m, 1H), 2.84 (dd, *J* = 12.9, 5.0 Hz, 1H), 2.64 (d, *J* = 12.6, 1H), 1.75–1.06 (m, 8H); ^{13}C NMR (126 MHz, $CDCl_3$) δ 172.1, 163.5, 145.5, 142.7, 133.8, 131.2, 129.8, 129.2, 128.4, 122.3, 66.1, 61.7, 60.0, 55.5, 46.0, 40.4, 33.1, 28.2, 28.0, 24.6; HRMS (ESI^+) calculated for $[C_{36}H_{44}N_6O_8S_3+Na]^+$ 807.2275, found 807.2301 (Δ −3.3 ppm).

4.2. Biological assays

4.2.1. Constructs, protein expression and purification

pET21 containing core streptavidin (SA),[47] core streptavidin with a C-terminal Glu_6 tag (SAe),[16] A86D streptavidin[48] and Dead streptavidin (D)[22] (the N23A, S27D, S45A mutant of core streptavidin showing negligible biotin binding) have been previously described. pET21 containing A86D core streptavidin with a C-terminal Glu_6 tag (A86D-SAe) was cloned by QuikChange from SAe, using primers previously described.[48] The A86D-SAe construct was verified by sequencing; GenBank Accession Number KJ401123. All streptavidin subunits were expressed in *Escherichia coli* and then refolded from inclusion bodies by dilution into PBS as previously described.[49] After refolding, the protein was first purified on iminobiotin-sepharose as described.[16] Monovalent streptavidin (SAe1D3), A86D monovalent streptavidin (A86D-SAe1D3), and 1,3 *trans*-divalent streptavidin (SAe2D2) were purified by ion-exchange chromatography.[16] All proteins were dialyzed into PBS and stored at 5–10 mg/mL. Protein concentrations were calculated from A_{280} via ProtParam. The concentrations of all the streptavidin forms refer to the concentration of monomer.

4.2.2. Crystallization and data collection

Crystals of the streptavidin/LH ligand complexes were obtained by the sitting drop crystallization method. Ligands were dissolved at 100 mM in DMSO. Briefly, 1 mM protein was incubated with 2 mM ligand for 1 h at rt in PBS with 10% DMSO. Samples were then centrifuged for 3 min at 17,000 g to remove any precipitate. 1 μL of the protein ligand solution was then mixed with varying amounts, 0.5–3 μL, of crystallization buffer (75% ammonium sulfate, 25% 1 M sodium acetate pH 4.5) in a sitting drop 2 well Swissci plate (Hampton Research). Crystals were typically obtained after a few hours at rt and reached a maximum size after 1–2 days. Crystals of A86D streptavidin with LH4 were obtained by mixing equal amounts of 1 mM protein with 2 mM LH4 in PBS with 30% 2-methyl-2,4-pentanediol (MPD). This stock was used to set up sitting drops in a 2 well Swissci plate with the best diffracting crystals (2 weeks at rt) obtained with condition A9 of the Morpheus screen: 0.1 M bicine/Trizma base pH 8.5, 10% w/v polyethylene glycol 20,000, 20% v/v polyethylene glycol monomethyl ether 550, 30 mM magnesium chloride and 30 mM calcium chloride.[50]

Prior to data collection, crystals were mounted and immersed into liquid nitrogen, using 6 M sodium formate as a cryoprotectant (LH1) or 30% MPD with 2 mM ligand (LH3 and LH4) for crystals obtained using ammonium sulfate. Crystals of A86D streptavidin bound to LH4 were frozen directly without further cryoprotectant. All crystallographic data were collected at the Diamond Light Source, Didcot, UK. Data for SA/LH1, *trans*-divalent SA/LH4 and A86D SA/LH4 were collected at 100 K at the IO2 beamline using a Pilatus 6 M detector and 0.98 Å wavelength beam. Data for SA/LH3 were collected at 100 K at the IO4 beamline using a Pilatus 6 M-f detector and 0.98 Å wavelength beam.

4.2.3. Structure solution and refinement

Data were auto-indexed and integrated using the xia2 program upon collection.[51] Structures were phased by molecular replacement from PDB 3RY1 (apo-streptavidin)[27] and further refined using Phenix,[52] through a Python graphical user interface. Models were altered to fit better the electron density using Coot.[53] Throughout refinement, all data were included from lowest to the highest resolution and anisotropic temperature factors were refined. Models were continually evaluated using MolProbity.[54] Crystallographic Information File (CIF) restraints for LH ligands were calculated using the GRADE server (Global Phasing Ltd): http://grade.globalphasing.org/cgi-bin/grade/server.cgi. Refinement statistics and other structure factors for the four structures are shown in Table 1. Structures were visualized and images for figures prepared using PyMOL (Schrödinger, LLC). Electron density maps were visualized and images prepared (contoured at 1 rmsd) with the CCP4 mg program.[55] Hydrogen bonds were determined in Coot,[53] with a 3.5 Å cut-off. 2mFo-DFc images, mFo-DFc images, and omit maps of the ligand in each structure are presented in Supplementary Figures S1, S3, S4 and S6. The electron density for residues 46–48 in the A86D streptavidin/LH4 structure was not clearly defined and these residues were modeled using standard stereochemical restraints in the subunit where LH4 ligand was clearly observed. In the A86D subunit where LH4 was only partially observed, 46–48 was not modeled. The coordinates and structure factors for the crystal structures been deposited in the Protein Data Bank with accession codes 4CPE for wild-type streptavidin with LH1, 4CPF for wild-type streptavidin with LH3, 4CPH for *trans*-divalent streptavidin with LH4, and 4CPI for A86D streptavidin with LH4. The best resolved ligand for each structure is bound to chain B (4CPE), chain B (4CPF), chain C (4CPH) and chain D (4CPI).

4.2.4. Biotin-4-fluorescein equilibrium assay

Monovalent streptavidin or A86D monovalent streptavidin (55 nM) was incubated for 1 h at rt with 11 nM biotin-4-fluorescein (Life Technologies) in 90 μL total volume. Then 10 μL of ligand at varying concentrations in DMSO was added and incubated for 48 h at 37 °C in closed PCR tubes. Samples were allowed to cool to rt for 1 h before being transferred to a black 96 well plate. The fluorescence increase of biotin-4-fluorescein upon unbinding from streptavidin[24] was monitored from λ_{ex} = 485 nm and λ_{em} = 520 nm using a PHERAstar FS plate reader (BMG Labtech). The percentage

dissociation was calculated as (signal with ligand − signal without ligand)/(signal without quenching − signal without ligand) × 100. The signal without quenching was taken as the biotin-4-fluorescein fluorescence in the absence of streptavidin. Experiments were repeated 3 times. Biotin, biocytin, desthiobiotin and (±)-α-lipoic acid were from Sigma-Aldrich and stocks prepared at 100 mM in DMSO. The one-site competitive binding fit was calculated using GraphPad Prism, giving an EC_{50} with 95% confidence intervals as well as a R^2 Pearson correlation coefficient value.

Acknowledgments

M.F. and M.H. were funded by the Biotechnology and Biological Sciences Research Council (BBSRC). E.D.L. was funded by the University of Oxford Department of Biochemistry. L.K.M.C. was funded by Oxford Synthesis Connections (OxSynC) from the University of Oxford and the Engineering and Physical Sciences Research Council (EPSRC). We thank Claire Chivers for cloning of A86D streptavidin.

Supplementary data

Supplementary data associated with this article can be found, in the online version, at http://dx.doi.org/10.1016/j.bmc.2014.07.029.

References and notes

1. Rago, F.; Cheeseman, I. M. *J. Cell Biol.* **2013**, *200*, 557.
2. Carey, S. P.; D'Alfonso, T. M.; Shin, S. J.; Reinhart-King, C. A. *Crit. Rev. Oncol. Hematol.* **2012**, *83*, 170.
3. Vogel, V.; Sheetz, M. P. *Curr. Opin. Cell Biol.* **2009**, *21*, 38.
4. Hoefer, I. E.; den Adel, B.; Daemen, M. J. *Cardiovasc. Res.* **2013**, *99*, 276.
5. Evans, E. A.; Calderwood, D. A. *Science* **2007**, *316*, 1148.
6. Grubmuller, H.; Heymann, B.; Tavan, P. *Science* **1996**, *271*, 997.
7. Dror, R. O.; Dirks, R. M.; Grossman, J. P.; Xu, H.; Shaw, D. E. *Annu. Rev. Biophys.* **2012**, *41*, 429.
8. Green, N. M. *Methods Enzymol.* **1990**, *184*, 51.
9. Rico, F.; Moy, V. T. *J. Mol. Recognit.* **2007**, *20*, 495.
10. Izrailev, S.; Stepaniants, S.; Balsera, M.; Oono, Y.; Schulten, K. *Biophys. J.* **1997**, *72*, 1568.
11. Laitinen, O. H.; Hytonen, V. P.; Nordlund, H. R.; Kulomaa, M. S. *Cell. Mol. Life Sci.* **2006**, *63*, 2992.
12. Sano, T.; Vajda, S.; Cantor, C. R. *J. Chromatogr. B Biomed. Sci. Appl.* **1998**, *715*, 85.
13. Weber, P. C.; Ohlendorf, D. H.; Wendoloski, J. J.; Salemme, F. R. *Science* **1989**, *243*, 85.
14. Stayton, P. S.; Freitag, S.; Klumb, L. A.; Chilkoti, A.; Chu, V.; Penzotti, J. E.; To, R.; Hyre, D.; Le Trong, I.; Lybrand, T. P.; Stenkamp, R. E. *Biomol. Eng.* **1999**, *16*, 39.
15. Zimbron, J. M.; Heinisch, T.; Schmid, M.; Hamels, D.; Nogueira, E. S.; Schirmer, T.; Ward, T. R. *J. Am. Chem. Soc.* **2013**, *135*, 5384.
16. Fairhead, M.; Krndija, D.; Lowe, E. D.; Howarth, M. *J. Mol. Biol.* **2014**, *426*, 199.
17. Wilbur, D. S.; Chyan, M. K.; Pathare, P. M.; Hamlin, D. K.; Frownfelter, M. B.; Kegley, B. B. *Bioconjug. Chem.* **2000**, *11*, 569.
18. Wilbur, D. S.; Hamlin, D. K.; Chyan, M. K. *Bioconjug. Chem.* **2006**, *17*, 1514.
19. Mei, T. S.; Giri, R.; Maugel, N.; Yu, J. Q. *Angew. Chem., Int. Ed.* **2008**, *47*, 5215.
20. Suau, R.; Rico, R.; Najera, F.; Ortiz-Lopez, F. J.; Lopez-Romero, J. M.; Moreno-Manas, M.; Roglans, A. *Tetrahedron* **2004**, *60*, 5725.
21. Gu, W.; Wang, S. F. *Eur. J. Med. Chem.* **2010**, *45*, 4692.
22. Howarth, M.; Chinnapen, D. J.; Gerrow, K.; Dorrestein, P. C.; Grandy, M. R.; Kelleher, N. L.; El Husseini, A.; Ting, A. Y. *Nat. Methods* **2006**, *3*, 267.
23. Gallivan, J. P.; Dougherty, D. A. *Proc. Natl. Acad. Sci. U.S.A.* **1999**, *96*, 9459.
24. Kada, G.; Falk, H.; Gruber, H. J. *Biochim. Biophys. Acta* **1999**, *1427*, 33.
25. Hirsch, J. D.; Eslamizar, L.; Filanoski, B. J.; Malekzadeh, N.; Haugland, R. P.; Beechem, J. M.; Haugland, R. P. *Anal. Biochem.* **2002**, *308*, 343.
26. Mock, D. M.; Nyalala, J. O.; Raguseo, R. M. *J. Nutr.* **2001**, *131*, 2208.
27. Le Trong, I.; Wang, Z.; Hyre, D. E.; Lybrand, T. P.; Stayton, P. S.; Stenkamp, R. E. *Acta Crystallogr. D Biol. Crystallogr.* **2011**, *67*, 813.
28. Hyre, D. E.; Le Trong, I.; Freitag, S.; Stenkamp, R. E.; Stayton, P. S. *Protein Sci.* **2000**, *9*, 878.
29. Chivers, C. E.; Koner, A. L.; Lowe, E. D.; Howarth, M. *Biochem. J.* **2011**, *435*, 55.
30. Plazuk, D.; Zakrzewski, J.; Salmain, M.; Blauz, A.; Rychlik, B.; Strzelczyk, P.; Bujacz, A.; Bujacz, G. *Organometallics* **2013**, *32*, 5774.
31. Wilbur, D. S.; Hamlin, D. K.; Chyan, M. K.; Kegley, B. B.; Pathare, P. M. *Bioconjug. Chem.* **2001**, *12*, 616.
32. Chivers, C. E.; Crozat, E.; Chu, C.; Moy, V. T.; Sherratt, D. J.; Howarth, M. *Nat. Methods* **2010**, *7*, 391.
33. Chu, V.; Freitag, S.; Le Trong, I.; Stenkamp, R. E.; Stayton, P. S. *Protein Sci.* **1998**, *7*, 848.
34. Le Trong, I.; Chu, V.; Xing, Y.; Lybrand, T. P.; Stayton, P. S.; Stenkamp, R. E. *Acta Crystallogr. D Biol. Crystallogr.* **2013**, *69*, 968.
35. Park, S. I.; Shenoi, J.; Frayo, S. M.; Hamlin, D. K.; Lin, Y.; Wilbur, D. S.; Stayton, P. S.; Orgun, N.; Hylarides, M.; Buchegger, F.; Kenoyer, A. L.; Axtman, A.; Gopal, A. K.; Green, D. J.; Pagel, J. M.; Press, O. W. *Clin. Cancer Res.* **2011**, *17*, 7373.
36. Dixon, R. W.; Radmer, R. J.; Kuhn, B.; Kollman, P. A.; Yang, J.; Raposo, C.; Wilcox, C. S.; Klumb, L. A.; Stayton, P. S.; Behnke, C.; Le Trong, I.; Stenkamp, R. *J. Org. Chem.* **1827**, *2002*, 67.
37. Le Trong, I.; Aubert, D. G.; Thomas, N. R.; Stenkamp, R. E. *Acta Crystallogr. D Biol. Crystallogr.* **2006**, *62*, 576.
38. Terai, T.; Maki, E.; Sugiyama, S.; Takahashi, Y.; Matsumura, H.; Mori, Y.; Nagano, T. *Chem. Biol.* **2011**, *18*, 1261.
39. Weber, P. C.; Wendoloski, J. J.; Pantoliano, M. W.; Salemme, F. R. *J. Am. Chem. Soc.* **1992**, *114*, 3197.
40. Pazy, Y.; Kulik, T.; Bayer, E. A.; Wilchek, M.; Livnah, O. *J. Biol. Chem.* **2002**, *277*, 30892.
41. Freitag, S.; Chu, V.; Penzotti, J. E.; Klumb, L. A.; To, R.; Hyre, D.; Le Trong, I.; Lybrand, T. P.; Stenkamp, R. E.; Stayton, P. S. *Proc. Natl. Acad. Sci. U.S.A.* **1999**, *96*, 8384.
42. DeChancie, J.; Houk, K. N. *J. Am. Chem. Soc.* **2007**, *129*, 5419.
43. Meenan, N. A.; Sharma, A.; Fleishman, S. J.; Macdonald, C. J.; Morel, B.; Boetzel, R.; Moore, G. R.; Baker, D.; Kleanthous, C. *Proc. Natl. Acad. Sci. U.S.A.* **2010**, *107*, 10080.
44. Liebeschuetz, J.; Hennemann, J.; Olsson, T.; Groom, C. R. *J. Comput. Aided Mol. Des.* **2012**, *26*, 169.
45. Kulhanek, J.; Pytela, O. *Collect. Czech. Chem. Commun.* **1997**, *62*, 913.
46. Aubineau, T.; Cossy, J. *Chem. Commun.* **2013**, *49*, 3303.
47. Sano, T.; Pandori, M. W.; Chen, X.; Smith, C. L.; Cantor, C. R. *J. Biol. Chem.* **1995**, *270*, 28204.
48. Crozat, E.; Meglio, A.; Allemand, J. F.; Chivers, C. E.; Howarth, M.; Venien-Bryan, C.; Grainge, I.; Sherratt, D. J. *EMBO J.* **2010**, *29*, 1423.
49. Howarth, M.; Ting, A. Y. *Nat. Protoc.* **2008**, *3*, 534.
50. Gorrec, F. *J. Appl. Crystallogr.* **2009**, *42*, 1035.
51. Winter, G. *J. Appl. Crystallogr.* **2010**, *43*, 186.
52. Terwilliger, T. C.; Grosse-Kunstleve, R. W.; Afonine, P. V.; Moriarty, N. W.; Zwart, P. H.; Hung, L. W.; Read, R. J.; Adams, P. D. *Acta Crystallogr. D Biol. Crystallogr.* **2008**, *64*, 61.
53. Emsley, P.; Lohkamp, B.; Scott, W. G.; Cowtan, K. *Acta Crystallogr. D Biol. Crystallogr.* **2010**, *66*, 486.
54. Davis, I. W.; Murray, L. W.; Richardson, J. S.; Richardson, D. C. *Nucleic Acids Res.* **2004**, *32*, W615–W619.
55. McNicholas, S.; Potterton, E.; Wilson, K. S.; Noble, M. E. *Acta Crystallogr. D Biol. Crystallogr.* **2011**, *67*, 386.